Regular Article

PHYSICAL CHEMISTRY RESEARCH
Published by the
Iranian Chemical Society
www.physchemres.org
info@physchemres.org

Phys. Chem. Res., Vol. 12, No. 3, 579-589, September 2024
DOI: 10.22036/pcr.2023.415502.2423

Discovery of a Potential Inhibitor Against Lung Cancer: Computational Approaches and Molecular Dynamics Study

El M. Karim, O. Abchir, H. Nour, I. Yamari, L. Bennani, M. EL Kouali, M. Talbi, A. Errougui and S. Chtita*

Laboratory of Analytical and Molecular Chemistry, Faculty of Sciences Ben M'Sik, Hassan II University of Casablanca, B. P 7955 Casablanca, Morocco

(Received 22 September 2023, Accepted 15 November 2023)

Lung cancer, the leading cause of cancer-related deaths globally, presents a formidable challenge due to delayed diagnoses and limited treatment options, contributing to persistently low five-year survival rates. This study aimed to identify a novel inhibitor for lung cancer through an exhaustive screening process. Initial exploration of a database containing over 500,000 molecules led to an ADME-Tox study, narrowing the selection down to 20,000 molecules. Subsequent molecular docking studies, employing SP and XP methods, revealed compelling candidates. From docking results, the top 250 molecules with significantly high docking scores were examined. Only two specific molecules, L3 with a notable docking score of -11.4 and L2 scoring -10.344, exhibited exceptional binding affinities compared to the reference compound (9FX), a recognized lung cancer inhibitor. These potent compounds displayed promising drug-like properties, boasting higher molecular weights (L2: 352.41 and L3: 341.36) compared to 9FX (342.35). Additionally, they showcased similar or superior LogP values (lipophilicity) and LogS values (aqueous solubility), signifying their potential for enhanced drug-like characteristics. Molecular dynamics (MD) simulations focusing on the protein-ligand complexes involving protein 5ZMA and the ligands L2 and L3 provided crucial insights. The simulations unveiled dynamic behaviors and potential adaptive structural changes within the protein-ligand complex. Notably, specific residues, particularly ILE-267 and LYS-494, demonstrated increased flexibility, potentially serving as pivotal hotspots for effective ligand binding or allosteric interactions. Our study identifies compounds L2 and L3 as strong contenders for lung cancer treatment. We propose advancing these compounds for further research and potential clinical trials.

Keywords: Virtual screening, Molecular dynamics, Schrodinger, Lung cancer, SP docking, XP docking

INTRODUCTION

Lung cancer continues to pose a significant public health challenge, contributing to high mortality rates across the globe [1]. Given the disease's widespread occurrence, aggressive nature, and limited treatment options, there is a pressing need for innovative approaches that can lead to improved patient outcomes and ultimately overcome this formidable disease [2]. One crucial aspect in the battle against lung cancer is early detection and timely intervention [3]. Identifying lung cancer at its earliest stages can significantly increase the chances of successful treatment and positive outcomes for patients [3]. However, due to the lack of specific symptoms in the early stages, lung cancer is often diagnosed at more advanced stages, making it difficult to treat effectively. Therefore, there is a critical need for improved diagnostic tools and strategies that can detect lung cancer at an early and potentially curable stage [4]. In addition to early detection, finding effective treatment options is essential [5]. Lung cancer is a complex disease with various subtypes and molecular pathways involved. Traditional treatment approaches such as chemotherapy and radiation therapy have limitations in terms of their effectiveness and potential side effects. Therefore,

*Corresponding author. E-mail: samirchtita@gmail.com

researchers are actively exploring novel therapeutic agents that specifically target the molecular pathways associated with lung cancer. These targeted therapies aim to disrupt the specific mechanisms that promote cancer growth and progression while minimizing harm to healthy cells [6]. However, the process of discovering and developing these targeted therapies can be time-consuming and costly. It typically involves screening large compound libraries to identify potential drug candidates, followed by extensive preclinical and clinical testing. This process can take several years and involves substantial financial investments [7]. Therefore, finding ways to expedite this process without compromising safety and efficacy is of utmost importance [8]. This is where computational methods come into play. By leveraging the power of computational tools and techniques, researchers can efficiently screen vast libraries of chemical compounds to identify potential drug candidates with desired properties for inhibiting lung cancer. These virtual screening techniques employ various algorithms and models to predict the likelihood of a compound binding to specific target proteins involved in lung cancer [9]. Once potential compounds have been identified, molecular docking techniques are employed to assess the strength and stability of the interactions between the selected compounds and the target proteins. Molecular docking simulations provide valuable insights into how the compounds fit into the three-dimensional structure of the target proteins and how tightly they bind. This information helps researchers prioritize and select the most promising candidates for further investigation [10]. Furthermore, molecular dynamics simulations are used to study the dynamic behavior of the selected compound-protein interactions over time. These simulations provide a detailed understanding of the complex's structural properties, flexibility, and stability. By exploring the complex's behavior at the molecular level, researchers can gain insights into its potential efficacy as a therapeutic agent and predict how it might interact with other components in the biological system [11]. The integration of computational approaches with traditional experimental techniques in the drug discovery process offers numerous advantages. It allows researchers to explore a significantly larger chemical space, saving time and resources by narrowing down the search for potential inhibitors. Computational methods also enable the identification of compounds with specific properties and mechanisms of action, potentially leading to more targeted and personalized treatment options [12]. Ultimately, the primary objective of utilizing computational tools in the quest for a potential inhibitor against lung cancer is to accelerate the drug discovery process. By efficiently screening compound libraries, performing molecular docking, and conducting molecular dynamics simulations, researchers can expedite the identification and development of novel drugs for lung cancer. These computational approaches hold great promise in advancing personalized treatment options and improving patient outcomes in the battle against this devastating disease [13]. In conclusion, lung cancer remains a significant public health challenge, but the integration of computational methods into the drug discovery process provides a cost-effective and efficient means to accelerate progress. Through virtual screening, molecular docking, and molecular dynamics simulations, researchers can narrow down the search space, gain valuable insights into the interactions between potential inhibitors and target proteins, and potentially uncover breakthrough treatments for lung cancer. These computational approaches offer hope for a future where personalized therapies and improved patient outcomes become a reality in the fight against lung cancer [14].

MATERIAL AND METHODS

Collection of Compound Database

A diverse set of compounds has been retrieved from PubChem, a comprehensive repository of chemical structures and bioactivity data [15]. The database provides a rich source of potential drug candidates for our study. The collected compounds undergo optimization using Schrödinger Maestro, a powerful software suite for molecular modeling and simulations, to improve their conformations [16]. The protonation state of each compound is determined, considering the pH conditions relevant to the target protein's binding pocket [17]. Additionally, stereoisomer generation is performed to explore the effects of chirality on molecular interactions. The compounds are assigned force field parameters using the OPLS3 force field [18]. This step ensures an accurate representation of the compounds' energetics and interactions during subsequent computational simulations.

Protein Preparation

The crystal structure of the target protein, with PDB ID: 5ZMA, is retrieved from the Protein Data Bank [19]. This protein is chosen based on its relevance to lung cancer and its known interactions with potential inhibitors. The retrieved protein structure undergoes refinement using Schrödinger Maestro [20]. This step involves correcting structural irregularities, optimizing hydrogen bonding, and removing any artifacts or non-standard residues to ensure a reliable protein model. Charges and bond orders are assigned to the protein structure, preparing it for subsequent molecular docking simulations. Accurate charge distributions are essential for capturing the electrostatic interactions between the protein and ligands. Water molecules and other solvent molecules are removed from the protein structure, as they can interfere with the docking process. Hydrogen atoms are added to the protein to restore correct bonding and improve accuracy during simulations. Hydrogen bond assignments within the protein structure are optimized to ensure the proper formation of critical interactions with potential ligands. Accurate hydrogen bonding patterns contribute to the reliability of docking results. The protein's amino acids are minimized using an appropriate force field at neutral pH conditions. This step optimizes the protein's conformation, reducing steric clashes and improving its overall stability [21].

Grid Box Generation

The receptor grid was created for the prepared protein [22]. The dimensions of the receptor grid box were set in each direction: (x = 28.64, y = 80.59, and z = 78.58) and the box was placed at the center of the binding pocket of the target protein. The grid box size was set to 20Å in each dimension (x, y, and z). The grid box defines the three-dimensional space within the protein's binding pocket where ligands will be docked, allowing efficient sampling of ligand conformations. The dimensions of the receptor grid are determined by analyzing the binding modes of known ligands within the protein's binding pocket. This ensures that the grid adequately covers the key interaction sites. The docking' box size is set to allow sufficient space for ligands to explore different orientations within the binding pocket. This facilitates a comprehensive sampling of ligand poses.

Molecular Dynamics Study

Molecular dynamics (MD) simulations are employed to investigate the dynamic behavior of the protein-ligand complex over time [27]. MD simulations utilize Newtonian physics principles to simulate the movements of atoms and molecules, providing insights into their stability, flexibility, and interactions. The protein-ligand complex obtained from the docking simulations is subjected to MD simulations to analyze its stability, flexibility, and molecular interactions [28]. This analysis helps determine the reliability of the binding mode and assess the complex's overall structural integrity. The MD simulations generate trajectories that reveal the behavior of the protein-ligand complex over time. By analyzing the conformational changes, intermolecular interactions, and binding dynamics, valuable insights are gained into the complex's behavior and its potential as a therapeutic target.

RESULTS AND DISCUSSION

Virtual Screening

Virtual screening is a computational technique used to screen large compound libraries and identify potential ligands that bind to a specific tar [23].

Docking SP

The prepared protein and the filtered compound database are subjected to molecular docking simulations using the Glide SP (Standard Precision) algorithm [24]. Docking scores are calculated to assess the binding affinity of each ligand towards the protein. Ligands with high docking scores, indicating favorable binding interactions with the protein, are identified as potential hits. We identified 250 molecules with high docking scores ranging from -10.019 to -8.077 (Table 1). These molecules exhibit promising binding affinity and are further analyzed for their drug-like properties.

Docking XP

To refine the search for potential inhibitors, a subset of top-scoring ligands from the SP docking is subjected to more accurate docking using the Glide XP (Extra Precision) algorithm [25]. XP docking provides a higher level of accuracy in predicting binding energies.

Table 1. The Binding Affinity of Docked Ligands in the 5ZMA Receptor Using Docking SP

Compound	Score (Kcal mol^{-1})	Compound	Score (Kcal mol^{-1})
L1	-9,658	L14	-8,685
L2	-9,313	L15	-8,663
L3	-9,188	L16	-8,663
L4	-9,182	L17	-8,577
L5	-9,075	L18	-8,567
L6	-9,065	L19	-8,556
L7	-8,968	L20	-8,518
L8	-8,852	L21	-8,478
L9	-8,79	L22	-8,443
L10	-8,769	L23	-8,434
L11	-8,711	L24	-8,427
L12	-8,704	L25	-8,366
L13	-8,688		

From the XP docking results, the top 250 molecules with the highest docking scores are selected as potential inhibitors. These compounds demonstrate strong binding affinity and favorable interactions with the target protein, suggesting their potential as effective inhibitors against lung cancer. Through the virtual screening process, two specific molecules are identified as potential inhibitors against lung cancer with significant docking score of L3: -11.4 and L2: -10.344 compared to the reference compound (9FX), which is a known lung cancer inhibitor (Table 2) [26]. These molecules exhibit exceptional binding affinities, favorable interactions with the target protein's binding pocket (Fig. 1), and promising drug-like properties.

Molecular Dynamics Results

We present a detailed discussion and interpretation of the molecular dynamics (MD) simulations performed on a potential inhibitor against lung cancer [29]. The simulations were carried out using Schrodinger software, and the resulting data includes protein-ligand RMSD, protein RMSF, and protein-ligand contacts. Through the analysis of these results, we gain valuable insights into the stability, flexibility, and molecular interactions within the complexes formed between the 5ZMA protein and ligands L2 and L3.

Table 2. The Binding Affinity of Docked Ligands in the 5ZMA Receptor Using Docking XP

Compound	Score (Kcal mol^{-1})
L3	-11,4
9FX	-10,852
L2	-10,344

Protein-Ligand RMSD

The protein-ligand RMSD plot provides information about the structural stability of the investigated complexes over time [30]. In the graphs shown in Fig. 2, the blue curve represents the RMSD of the protein backbone (C alpha), while the red curves correspond to the RMSD of the ligands L2 and L3. The Y-axis denotes the RMSD values in angstroms, and the X-axis represents the simulation time in nanoseconds. The red curve, depicting the ligand L2 RMSD, shows a relatively steady pattern, with the RMSD starting from 0 and stabilizing at around 2 Å until 20 ns. This initial stability suggests that the initial binding conformation is maintained during this period. However, after 20 ns, the ligand L2 experiences a sudden increase in RMSD, reaching up to 5 Å at approximately 45 ns. This increase indicates a significant conformational change or a potential binding event that affects the structural stability of the ligand.

Subsequently, from 45 ns to 65 ns, the ligand L2 shows a period of stabilization with minor fluctuations, suggesting that it adopts a new stable conformation. However, from 65 ns to 90 ns, the ligand L2 exhibits another increase in RMSD, reaching up to 7.5 Å. This pattern of increasing RMSD with a zigzag shape indicates further structural changes or potential dynamic interactions. Finally, from 95 ns to 100 ns, the ligand L2 returns to a stable position at 5 Å.

For the ligand L3, the red curve starts from 0 and stabilizes at 2 Å until 20 ns, similar to ligand L2. This initial stability suggests that the initial binding conformation of L3 is also maintained during this period. However, at approximately 45 ns, the RMSD of ligand L3 increases,

9FX

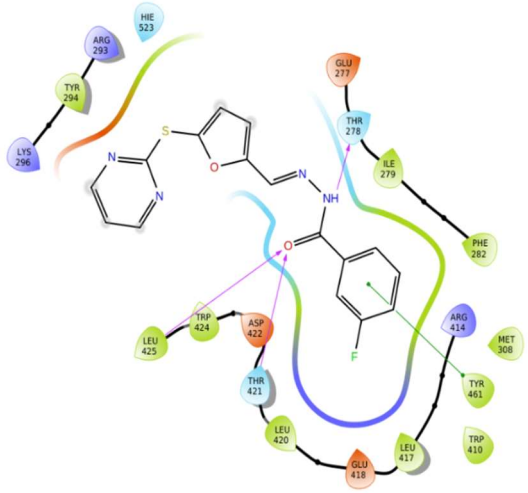

L2

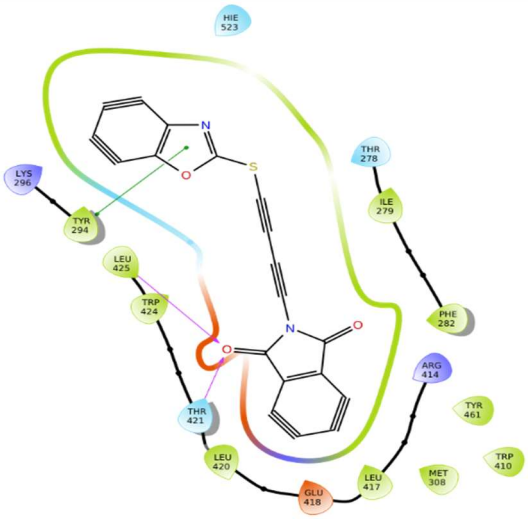

L3

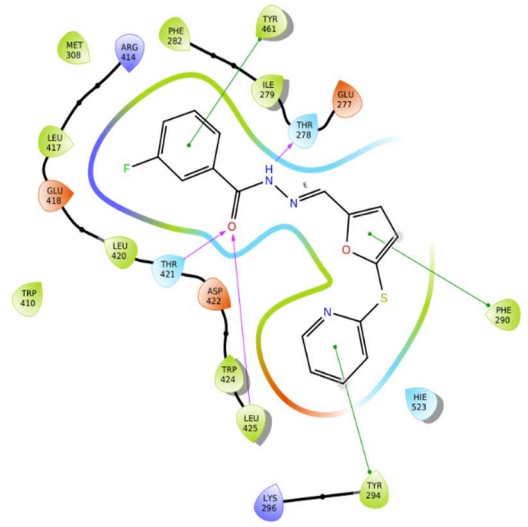

Fig. 1. 2D structures of formed complexes between analyzed compounds, reference compound, and 5ZMA receptor.

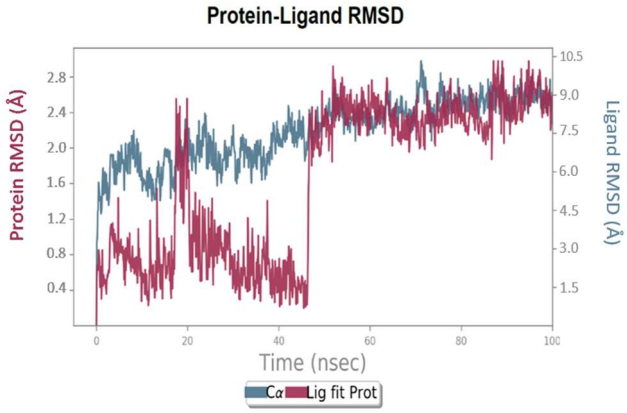

L2

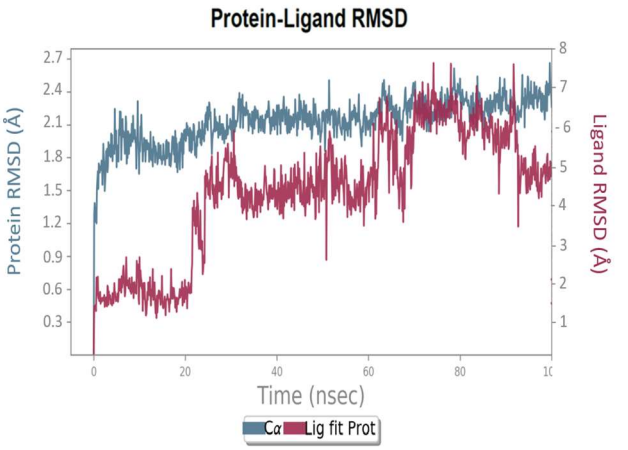

L3

Fig. 2. RMSD plots of complexes with ligands L2 and L3.

reaching up to 5 Å. This increase indicates a conformational change or potential binding event that affects the structural stability of L3. Following this, from 45 ns to 65 ns, ligand L3 stabilizes with minor fluctuations. However, from 65 ns to 90 ns, ligand L3 exhibits an increase in RMSD, reaching up to 7.5 Å, similar to ligand L2. This pattern of increasing RMSD with a zigzag shape suggests further dynamic behavior. Finally, from 95 ns to 100 ns, ligand L3 returns to a stable position at 5 Å, similar to ligand L2. These observations suggest that both ligands L2 and L3 undergo conformational changes or binding events that affect their structural stability during the simulation. These dynamic changes in RMSD highlight the potential flexibility and

adaptability of the ligands within the protein-ligand complex [31].

Protein RMSF

The protein RMSF plot provides insights into the flexibility of individual residues within the protein [32]. The RMSF plots of the investigated complexes are presented in Fig. 3. The Y-axis represents the RMSF values, which indicate the degree of fluctuation or mobility for each residue, ranging from 0 to 4.5 Å. The X-axis corresponds to the residue index, ranging from 0 to 250. Starting from the maximum value of 5.4 Å, the RMSF decreases steadily until around residue index 10, where it reaches a minimum of 0.6 Å. This initial decrease in RMSF suggests that the protein backbone and residues in the vicinity of the ligand-binding site exhibit lower fluctuations and higher stability. Following this minimum, the plot shows minor fluctuations, with occasional peaks reaching up to 1.9 Å. These fluctuations indicate the inherent flexibility of the protein residues, which may be involved in accommodating ligand binding or allosteric interactions. Notably, at residue index 55 (ILE-267), a significant increase in RMSF (3.9 Å) is observed. This observation suggests that residue ILE-267 exhibits higher flexibility and mobility compared to other residues. The increased flexibility in this region may be essential for ligand binding or for inducing conformational changes in nearby residues. Similarly, at residue index 80 (LYS-494), there is a noticeable increase in RMSF (3.7 Å), indicating increased mobility. This region of higher flexibility may also play a role in ligand recognition or binding. These regions of increased flexibility at residue indices 55 and 80 may serve as potential hotspots for ligand binding or allosteric interactions. The ability of these residues to undergo significant fluctuations suggests their importance in the dynamic behavior of the protein-ligand complex [33].

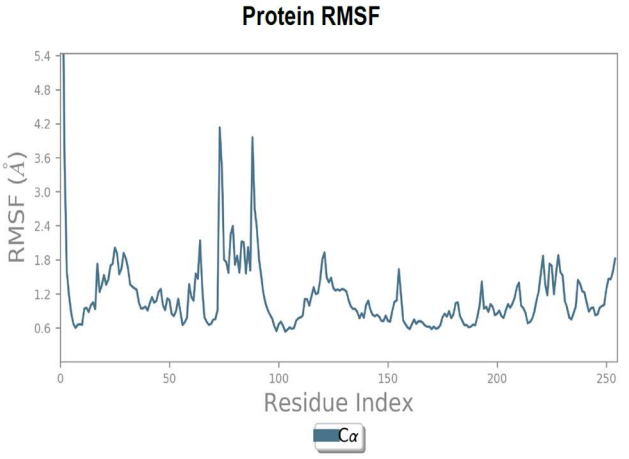

L2

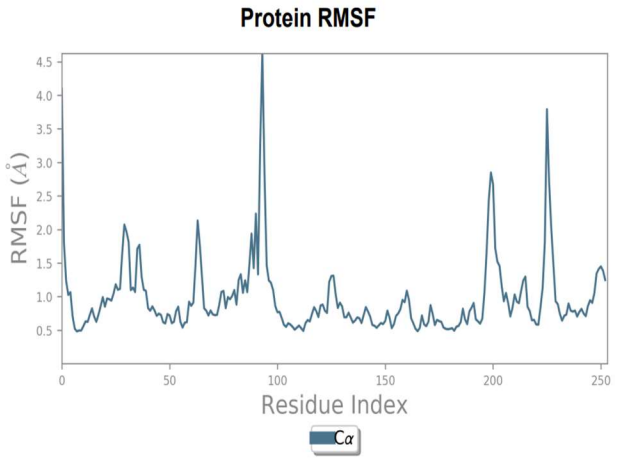

L3

Fig. 3. RMSF plots of complexes of target protein with ligands L2 and L3.

Protein-Ligand Contacts

The protein-ligand contacts graph provides information on the nature and frequency of interactions between specific amino acids and the ligand. The protein-ligands contacts are highlighted in Fig. 4. The Y-axis represents the interaction fraction, ranging from 0 to 0.30, while the X-axis displays the 15 selected amino acids. Most of the amino acids predominantly exhibit water bridges as the majority interaction type, followed by hydrogen bonds. Interestingly, only one amino acid, ALA_495, shows hydrophobic and hydrogen bond interactions. Moreover, the majority of the amino acids exhibit interaction fractions below 0.10, indicating weak or transient interactions. However, two residues stand out: ILE_267 with an interaction fraction of 0.25 and LYS_494 with an interaction fraction of 0.33. These residues exhibit a relatively higher affinity towards the ligand, suggesting potential key binding sites. Additionally, ALA_495, with an interaction fraction of 0.15, also shows a significant involvement in ligand binding. L3 was also investigated for protein-ligand contacts. The analysis

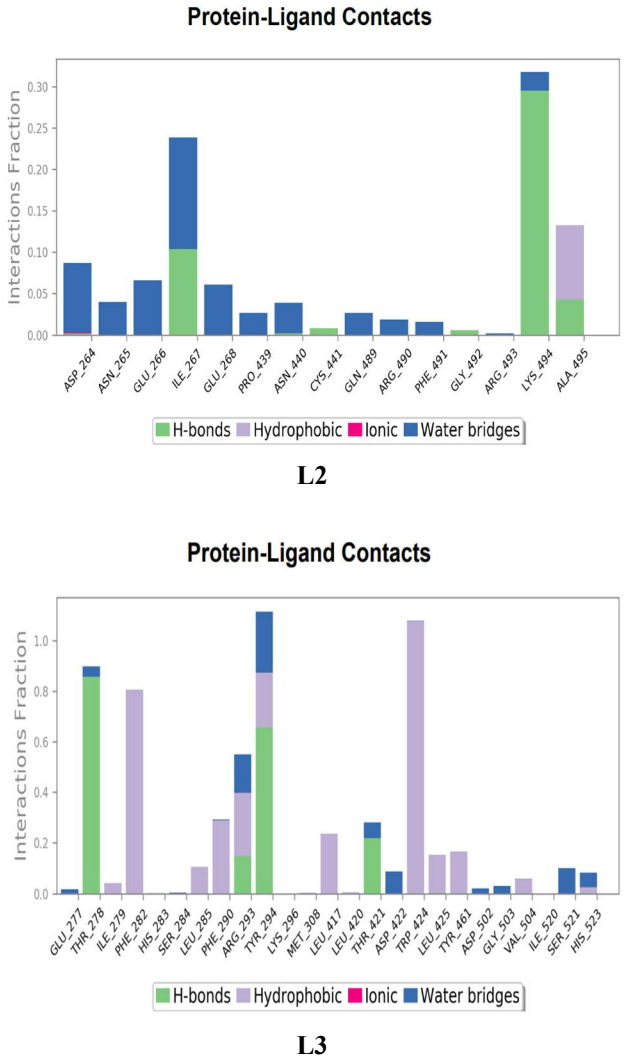

Fig. 4. Protein interactions with the ligands L2 and L3 throughout the simulation.

revealed various interaction types between the ligand and specific amino acids.

For L3, the protein-ligand contacts showed a predominance of hydrophobic interactions, particularly at TRP_424 with an interaction fraction of 1.1 and PHE_282 with an interaction fraction of 0.8. Additionally, H-bonds were observed at THR_278 with an interaction fraction of 0.9, and minor water bridges were present. Notably, TYR_294 exhibited a mixture of H-bonds, hydrophobic interactions, and water bridges, with an interaction fraction of 1.2. The protein-ligand contacts graph provides valuable insights into the nature and frequency of interactions, shedding light on the binding characteristics of L3 with the selected amino acids.

DISCUSSION

The molecular dynamics (MD) simulations presented in this study provide valuable insights into the behavior and interactions of the protein-ligand complex formed by protein 5ZMA and ligands L2 and L3 [34]. The analysis of the protein-ligand RMSD reveals interesting patterns in the stability of the complex over time. The initial stability observed for both ligands suggests that the initial binding conformation is maintained during the initial simulation period. However, subsequent increases in RMSD indicate significant conformational changes or potential binding events that affect the structural stability of the ligands. The zigzag pattern of increasing RMSD followed by periods of stabilization suggests dynamic behavior and the potential for adaptive structural changes within the protein-ligand complex. The protein RMSF analysis provides insights into the flexibility of individual residues within the protein. The observed fluctuations in RMSF indicate inherent flexibility and mobility of the protein residues. Residue indices 55 and 80, corresponding to ILE-267 and LYS-494, respectively, exhibit increased flexibility compared to other residues. These regions may serve as potential hotspots for ligand binding or allosteric interactions. The ability of these residues to undergo significant fluctuations suggests their importance in the dynamic behavior of the protein-ligand complex. The analysis of protein-ligand contacts reveals the nature and frequency of interactions between specific amino acids and the ligands. Most amino acids predominantly exhibit water bridges and hydrogen bonds as the major interaction types. However, two residues, ILE_267 and LYS_494, stand out with relatively higher interaction fractions, indicating a stronger affinity towards the ligands. These residues may play a crucial role in ligand binding and stabilization within the protein-ligand complex. Additionally, ALA_495 also shows significant involvement in ligand binding. For ligand L3, analysis of protein-ligand contact highlights hydrophobic interactions as the predominant interaction type. Specific

amino acids, such as TRP_424 and PHE_282, exhibit high interaction fractions, suggesting their importance in the binding characteristics of L3. H-bonds and minor water bridges are also observed, further contributing to the binding interactions between the ligand and selected amino acids. Overall, the MD simulations provide valuable insights into the stability, flexibility, and molecular interactions within the protein-ligand complex. These findings offer a deeper understanding of the complex's behavior and provide a foundation for further optimization and development of potential inhibitors for lung cancer [35].

ADME-Tox Analysis

In our study, we conducted a comprehensive ADME-Tox analysis to compare the reference compound, which is a known lung cancer inhibitor, with our newly identified candidates. Both new molecules and the reference molecule revealed similar properties with no significant violations in Lipinski, Ghose, Veber, Egan, and Muegge rules [36]. Therefore, the new compounds demonstrated lower molecular weight and lipophilicity, better solubility, and similar synthetic accessibility compared to the reference molecule.

To compare the ADMET (Absorption, Distribution, Metabolism, Excretion, and Toxicity) properties of the reference compound 9FX with ligands L2 and L3, we will focus on key parameters such as molecular weight (MW), LogP, LogS, solubility, and various inhibitory properties. Below is a Table 3 summarizing the values for these properties:

Ligands L2 and L3 exhibit several favorable properties compared to the reference compound 9FX [37]. Firstly, both ligands have slightly higher molecular weights (L2: 352.41 and L3: 341.36) compared to 9FX (342.35). Generally, higher MW is desirable as it enhances the chances of binding to the target. Additionally, both ligands possess similar or better LogP values (lipophilicity) and LogS values (aqueous solubility) compared to 9FX, indicating their potential for favorable drug-like properties. Moreover, L2 and L3 exhibit improved inhibitory profiles against several cytochrome P450 (CYP) enzymes (CYP1A2, CYP2C19, CYP2C9, CYP2D6, and CYP3A4) compared to 9FX. This suggests that L2 and L3 may have stronger inhibitory effects on these enzymes, which can be advantageous for drug metabolism and potential drug-drug interaction avoidance. In terms of ADMET-related properties, all three compounds demonstrate high gastrointestinal (GI) absorption, indicating good bioavailability. Notably, L3 possesses BBB permeability, suggesting its ability to cross the blood-brain barrier, which can be beneficial for targeting central nervous system-related diseases. Additionally, ligand L2 is identified as a P-glycoprotein (Pgp) substrate, indicating its potential to be transported out of cells by this efflux pump. This characteristic can be advantageous for drug delivery and distribution in certain scenarios. Both ligands L2 and L3 exhibit a comparable number of Lipinski and Veber violations to 9FX, indicating that they are within the acceptable range for drug-likeness and oral bioavailability. Considering these findings, ligands L2 and L3 present several advantages over the reference compound 9FX, such as improved inhibitory profiles, comparable or better ADMET properties, and favorable MW ranges. These factors make ligands L2 and L3 promising candidates for further

Table 3. Comparison of ADMET Properties: 9FX *vs*. Ligands L2 and L3

Property	9FX	L2	L3
MW	342.35	352.41	341.36
LogP	3.35	3.34	3.90
LogS	-4.20	-4.59	-4.60
Solubility (mg ml^{-1})	0.0215	0.009	0.0085
CYP1A2 Inhibitor	Yes	Yes	Yes
CYP2C19 Inhibitor	Yes	Yes	Yes
CYP2C9 Inhibitor	No	Yes	Yes
CYP2D6 Inhibitor	No	Yes	Yes
CYP3A4 Inhibitor	Yes	Yes	Yes
GI Absorption	High	High	High
BBB Permeant	No	No	Yes
Pgp Substrate	No	Yes	Yes
Lipinski Violations	0	0	0
Veber Violations	0	0	0
Synthetic Accessibility	3.12	2.93	3.31

exploration and potential selection as lung cancer inhibitors [38].

CONCLUSION

The study aimed to discover a potential inhibitor against lung cancer using computational approaches, encompassing data collection, compound and protein preparation, virtual screening, as well as molecular docking and dynamics simulations. The identified potential inhibitors demonstrate robust binding affinity, favorable interactions, and promising drug-like properties, positioning them as candidates for further investigation and potential development as lung cancer therapeutics. The findings offer valuable insights into the application of computational approaches in lung cancer drug discovery. They not only contribute to the ongoing efforts in the field but also open avenues for future research. However, the path ahead involves critical steps for translation and practical implementation. Moving forward, it is pivotal to proceed with experimental validation, optimizing the identified compounds, and further developing these novel therapeutic agents. The advancement of these compounds into clinical trials will be essential for assessing their efficacy, safety, and dosage in real-world settings. Moreover, additional computational studies, structural modifications, and toxicological assessments are warranted to propel these findings toward tangible clinical applications. These findings serve as a foundation for future investigations and drug development, marking a significant step forward in the fight against lung cancer. The integration of computational techniques with experimental validation not only holds promise for identifying targeted and effective treatments but also demonstrates the potential to improve patient outcomes in the battle against this devastating disease. In conclusion, this comprehensive study provides a strong basis for the future development of potential lung cancer inhibitors. The identified compounds, L2 and L3, demonstrate substantial potential, yet their realization into effective therapeutic agents necessitates further exploration, collaboration, and rigorous evaluation. This research underscores the significance of continued exploration in lung cancer therapeutics and offers a pathway toward more effective treatments and improved patient care.

REFERENCES

[1] Miller, K. D.; Nogueira, L.; Mariotto, A. B.; Rowland, J. H.; Yabroff, K. R.; Alfano, C. M.; Siegel, R. L., Cancer treatment and survivorship statistics, *CA Cancer J. Clin.* **2022**, *72* (5), 409-436, DOI: 10.3322/caac.21565.

[2] Siegel, R. L.; Miller, K. D.; Jemal, A., Cancer statistics, *CA Cancer J. Clin.* **2018**, *68* (1*)*, 7-30, DOI: 10.3322/caac.21442.

[3] Lindeman, N. I.; Cagle, P. T.; Beasley, M. B.; Chitale, D. A.; Dacic, S.; Giaccone, G.; Ladanyi, M., Molecular testing guideline for selection of lung cancer patients for EGFR and ALK tyrosine kinase inhibitors: guideline from the College of American Pathologists, International Association for the Study of Lung Cancer, and Association for Molecular Pathology, *J. Thorac. Oncol.* **2013**, *8* (7), 823-859, DOI: 10.1097/JTO.0b013e318290868f.

[4] Langer, C. J., Emerging immunotherapies in the treatment of non-small cell lung cancer (NSCLC): the role of immune checkpoint inhibitors, *Am. J. Clin. Oncol.* **2015**, *38* (4), 422-430, DOI: 10.1097/COC.0000000000000059.

[5] Barlesi, F.; Mazières, J.; Merlio, J. P.; Debieuvre, D.; Mosser, J.; Léna, H.; Zalcman, G., Routine molecular profiling of patients with advanced non-small-cell lung cancer: results of a 1-year nationwide programme of the French Cooperative Thoracic Intergroup (IFCT), *Lancet* **2016**, *387* (10026), 1415-1426, DOI: 10.1016/S0140-6736(16)00004-0.

[6] Guven, D. C.; Sahin, T. K.; Dizdar, O.; Kilickap, S., Predictive biomarkers for immunotherapy efficacy in non-small-cell lung cancer: current status and future perspectives, *Biomark. Med.* **2020**, *14* (14), 1383-1392, DOI: 10.2217/bmm-2020-0310.

[7] Al-Lazikani, B.; Banerji, U.; Workman, P., Combinatorial drug therapy for cancer in the post-genomic era, *Nat. Biotechnol.* **2012**, *30* (7), 679-692, DOI: 10.1038/nbt.2284.

[8] Li, J.; Fu, A.; Zhang, L., An overview of scoring functions used for protein-ligand interactions in molecular docking, *Interdiscip. Sci.* **2019**, *11*, 320-328, DOI: 10.1007/s12539-019-00327-w.

[9] Durrant, J. D.; McCammon, J. A., Molecular dynamics simulations and drug discovery, *BMC Biol.* **2011**, *9* (1), 1-9, DOI: 10.1186/1741-7007-9-71.

[10] Leelananda, S. P.; Lindert, S., Computational methods in drug discovery, *Beilstein J. Org. Chem.* **2016**, *12* (1), 2694-2718, DOI: 10.3762/bjoc.12.267.

[11] Laraia, L.; McKenzie, G.; Spring, D. R.; Venkitaraman, A. R.; Huggins, D. J., Overcoming chemical, biological, and computational challenges in the development of inhibitors targeting protein-protein interactions, *Chem. Biol.* **2015**, *22* (6), 689-703, DOI: 10.1016/j.chembiol.2015.04.019.

[12] Broadbelt, L. J.; Snurr, R. Q., Applications of molecular modeling in heterogeneous catalysis research, *Appl. Catal. A: Gen.* **2000**, *200* (1-2), 23-46, DOI: 10.1016/S0926-860X(00)00648-7.

[13] McInnes, C., Virtual screening strategies in drug discovery, *Curr. Opin. Chem. Biol.* **2007**, *11* (5), 494-502, DOI: 10.1016/j.cbpa.2007.08.033.

[14] UniProt Consortium, UniProt: a worldwide hub of protein knowledge, *Nucleic Acids Res.* **2019**, *47* (D1), D506-D515, DOI: 10.1093/nar/gky1049.

[15] PubChem. Retrieved from https://pubchem.ncbi.nlm.nih.gov/.

[16] Schrödinger Maestro. Retrieved from https://www.schrodinger.com/maestro.

[17] Li, H.; Robertson, A. D.; Jensen, J. H., Very fast empirical prediction and rationalization of protein pKa values, *Proteins: Struct. Funct. Bioinf.* **2005**, *61* (4), 704-721, DOI: 10.1002/prot.20660.

[18] Harder, E.; Damm, W.; Maple, J.; Wu, C.; Reboul, M.; Xiang, J. Y.; Friesner, R. A., OPLS3: a force field providing broad coverage of drug-like small molecules and proteins, *J. Chem. Theory Comput.* **2016**, *12* (1), 281-296, DOI: 10.1021/acs.jctc.5b00864.

[19] Protein Data Bank. Retrieved from https://www.rcsb.org/.

[20] Jacobson, M. P.; Pincus, D. L.; Rapp, C. S.; Day, T. J.; Honig, B.; Shaw, D. E.; Friesner, R. A., A hierarchical approach to all-atom protein loop prediction, *Proteins: Struct. Funct. Bioinf.* **2004**, *55* (2), 351-367, DOI: 10.1002/prot.10613.

[21] Zou, J.; Yin, J.; Fang, L.; Yang, M.; Wang, T.; Wu, W.; Zhang, P., Computational prediction of mutational effects on SARS-CoV-2 binding by relative free energy calculations, *J. Chem. Inf. Model.* **2020**, *60* (12), 5794-5802, DOI: 10.1021/acs.jcim.0c00679.

[22] Yamari, I.; Abchir, O.; Mali, S. N.; Errougui, A.; Talbi, M.; El Kouali, M.; Chtita, S., The anti-SARS-CoV-2 activity of novel 9,10-dihydrophenanthrene derivatives: an insight into molecular docking, ADMET analysis, and molecular dynamics simulation, *Sci. Afr.* **2023**, DOI: 10.1016/j.sciaf.2023.e01754.

[23] Kitchen, D. B.; Decornez, H.; Furr, J. R.; Bajorath, J., Docking and scoring in virtual screening for drug discovery: methods and applications, *Nat. Rev. Drug Discov.* **2004**, *3* (11), 935-949, DOI: 10.1038/nrd1549.

[24] Friesner, R. A.; Murphy, R. B.; Repasky, M. P.; Frye, L. L.; Greenwood, J. R.; Halgren, T. A.; Mainz, D. T., Extra precision glide: Docking and scoring incorporating a model of hydrophobic enclosure for protein-ligand complexes, *J. Med. Chem.* **2006**, *49(21)*, 6177-6196, DOI: 10.1021/jm051256o.

[25] Daoui, Ossama; Souad Elkhattabi; and Samir Chtita, Design and prediction of ADME/Tox properties of novel magnolol derivatives as anticancer agents for NSCLC using 3D-QSAR, molecular docking, MOLCAD and MM-GBSA studies, *Lett. Drug Des. Discov.* **2023**, *20* (5), 545-569, DOI: 10.2174/1570180819666220510141710.

[26] Chalkha, M.; Nour, H.; Chebbac, K.; Nakkabi, A.; Bahsis, L.; Bakhouch, M.; Akhazzane, M.; Bourass, M.; Chtita, S.; Bin Jardan, Y. A.; Augustyniak, M.; Bourhia, M.; Aboul-Soud, M. A. M.; El Yazidi, M., Synthesis, Characterization, DFT Mechanistic Study, Antimicrobial Activity, Molecular Modeling, and ADMET Properties of Novel Pyrazole-isoxazoline Hybrids, *ACS Omega* **2022**, *7* (50), 46731-46744, DOI: 10.1021/acsomega.2c05788.

[27] Ryazantsev, M. N.; Strashkov, D. M.; Nikolaev, D. M.; Shtyrov, A. A.; Panov, M. S., Photopharmacological compounds based on azobenzenes and azoheteroarenes: Principles of molecular design, molecular modelling, and synthesis, *Russ. Chem. Rev.* **2021**, *90* (7), 868, DOI: 10.1070/RCR5001.

[28] Karplus, Martin; J. Andrew McCammon, Molecular dynamics simulations of biomolecules, *Nat. Struct.*

Mol. Biol. **2002**, *9* (9), 646-652, DOI: 10.1038/nsb0902-646.

[29] Abchir, O.; Yamari, I.; Nour, H.; Daoui, O.; Elkhattabi, S.; Errougui, A.; Chtita, S., Structure-Based Virtual Screening, ADMET analysis, and Molecular Dynamics Simulation of Moroccan Natural Compounds as Candidates α-Amylase Inhibitors, *ChemistrySelect* **2023**, *8* (26), e202301092, DOI: 10.1002/slct.202301092.

[30] Lindorff-Larsen, K.; Piana, S.; Palmo, K.; Maragakis, P.; Klepeis, J. L.; Dror, R. O.; Shaw, D. E., Improved side-chain torsion potentials for the Amber ff99SB protein force field, *Proteins: Struct. Funct. Bioinf.* **2010**, *78* (8), 1950-1958, DOI: 10.1002/prot.22711.

[31] Ollila, OH Samuli; Harri A., Heikkinen; Hideo Iwaï, Rotational dynamics of proteins from spin relaxation times and molecular dynamics simulations, *J. Phys. Chem. B* **2018**, *122* (25), 6559-6569, DOI: 10.1021/acs.jpcb.8b02250.

[32] Robustelli, Paul; Stefano Piana; David E. Shaw, Developing a molecular dynamics force field for both folded and disordered protein states, *Proc. Natl. Acad. Sci.* **2018**, *115* (21), E4758-E4766, DOI: 10.1073/pnas.1800690115.

[33] Drew, Elliot D.; Robert W. Janes, PDBMD2CD: providing predicted protein circular dichroism spectra from multiple molecular dynamics-generated protein structures, *Nucleic Acids Res.* **2020**, *48* (W1), W17-W24, DOI: 10.1093/nar/gkaa296.

[34] Huang, Jing; Alexander D. MacKerell Jr., Force field development and simulations of intrinsically disordered proteins, *Curr. Opin. Struct. Biol.* **2018**, *48*, 40-48, DOI: 10.1016/j.sbi.2017.10.008.

[35] Salo-Ahen, O. M. H.; Alanko, I.; Bhadane, R.; Bonvin, A. M. J. J.; Honorato, R. V.; Hossain, S.; Juffer, A. H.; Kabedev, A.; Lahtela-Kakkonen, M.; Larsen, A. S.; Lescrinier, E.; Marimuthu, P.; Mirza, M. U.; Mustafa, G.; Nunes-Alves, A.; Pantsar, T.; Saadabadi, A.; Singaravelu, K.; Vanmeert, M., Molecular dynamics simulations in drug discovery and pharmaceutical development," *Processes* **2020**, *9* (1), 71, DOI: 10.3390/pr9010071.

[36] Lipinski, C. A.; Lombardo, F.; Dominy, B. W.; Feeney, P. J., Experimental and computational approaches to estimate solubility and permeability in drug discovery and development settings, *Adv. Drug Deliv. Rev.* **1997**, *23* (1-3), 3-25, DOI: 10.1016/S0169-409X(96)00423-1.

[37] Abchir, O.; Daoui, O.; Nour, H.; Yamari, I.; Elkhattabi, S.; Errougui, A.; Chtita, S., Cannabis constituents as potential candidates against diabetes mellitus disease using molecular docking, dynamics simulations, and ADMET investigations, *Sci. Afr.* **2023**, DOI: 10.1016/j.sciaf.2023.e01745.